A Multi-Layer Commingled Composite Reservoir Model for Thermal Well Test Analysis

Ashkan Jahanbani G.[#1], Tom A. Jelmert[#2]

[#1,2] *Department of Petroleum Engineering and Applied Geoscience, Norwegian University of Science and Technology (NTNU) S.P. Andersens vei 15 A, 7491 Trondheim, Norway*

Abstract— Many enhanced oil recovery projects like steam injection into an oil reservoir are analyzed using composite reservoir models. Most of the models used assume two-region composite reservoirs with highly different properties separated by a vertical front. Applicability of thermal well test analysis method was evaluated previously using simulation studies of both vertical and horizontal steam injection wells with the conclusion that simplifying assumptions of the conventional two-region models may not explain some pressure behavior and may cause significant errors in the estimates. The main objective of this paper is therefore to develop a new analytical model for well test analysis to improve previous models. The model is a three-region composite model with an intermediate region characterized by power-law decline of properties. Fronts are tilted due to the gravity override and are modeled using the multi-layer reservoir concept assigning different front radii to each layer. A commingled model is assumed in which there is no cross-flow between the layers and all the communication happens through the wellbore. Steam condensation is included in the form of heat loss to the formation. Pressure type curves are generated and validated. Effects of the important parameters included in the model are investigated. The model developed in this work will be used in type curve matching for improved well test analysis.

Keywords— commingled system, composite reservoir, gravity override, heat loss, multi-layer, thermal well test

I. INTRODUCTION

Well test analysis is a deconvolution or inverse solution. The input (for example change of flow rate) and the output (for example pressure data) are known, and the objective is to characterize and identify the system (reservoir properties) by matching the obtained data to the model type curves. Selection of the model is very important. A composite reservoir may be formed artificially by applying enhanced oil recovery (EOR) methods such as steam injection for reducing the viscosity of oil or cold water injection into a hot oil reservoir. Radial composite reservoirs have been investigated since early 1960's (for instance in [1] and [2]).

In most of the EOR projects and specifically steam injection, the composite model developed in [3] is used for the analysis of data. The analysis method (also called pseudo-steady-state or PSS method) assumes a model consisting of two regions, each defined by its particular rock and/or fluid properties that are highly different from the other region to model the condition of an impermeable boundary at the front location. Due to the irregularity in the shape, it is better to express the front radius in terms of swept volume.

Fall off test analysis offers an inexpensive and quick method for estimation of the swept volume which is very important for assessing the success of a project and thermal efficiencies in thermal processes. Reference [4] introduced the use of pressure falloff data to approximate the location of a burning front in an in-situ combustion process.

The two-region simplification of composite reservoirs was improved by analytical two, three and multi-region composite reservoir models ([5]-[13]). Reference [14] used the fractal concept for property variation in the intermediate-region of their three-region model to account for gradual change of properties.

To model a tilted front due to gravity effects or various shapes of fronts formed due to viscous fingering, multi-layered reservoir model is used. A reservoir model in which there is no vertical flow between layers is referred to as a commingled system. In the case of inter-layer communication, the reservoir is called a layered system with cross-flow. Reference [15] studied the behaviour of commingled systems composed of n-layers, each with distinct properties. They presented both pressure and layer flow rate transient responses for analyzing bounded reservoir characteristics. Application of multi-layer models was extended to composite reservoirs (as in [16] and [17]) to study the effects of a tilted front. These references presented pressure responses for a commingled, multi-layered composite system with tilted front. References [18] and [19] presented pressure solution for interference in a two-layer model with cross-flow. A general analytical solution for multi-layered composite reservoir with formation cross-flow was presented in [20]. To best of our knowledge, not much analytical work has been done in this field since then. Regarding horizontal wells, recently a few simulation studies have been reported ([21] and [22]).

The application of thermal well testing method to different cases was investigated in some initial simulation studies to consider some fundamental concepts and to evaluate the applicability and accuracy of thermal well test analysis method and the effects of several parameters on the results ([23]-[25]). Errors in some cases are reported significant and there are trends on the pressure plots which cannot be explained correctly using the existing models. It is therefore intended in this paper to develop an analytical model for the pressure behaviour of a three-region composite model with power-law variation of properties in the intermediate region. Gravity override is modelled using the concept of multi-layer system. Each layer acts like a composite reservoir having

three regions with different front radii resulting in a tilted front. Steam condensation is included in the model by considering heat loss from the steam zone to the overburden and underburden.

The proposed model is validated and a sensitivity study to the parameters included in the model is done using the pressure derivative responses. This model will update the previous composite reservoir models with inclusion of additional parameters and more realistic assumptions.

II. Mathematical Model

Unlike the traditional composite model assumption, in reality and in most of the cases studied in [23]-[25], three zones are formed: steam zone, hot water zone and the cold oil zone. A three-region model is introduced in this section. The following assumptions are applied:

1) Slightly compressible fluid (small compressibility)
2) Isotropic porous medium
3) Small pressure gradient
5) Radial flow
6) Applicability of Darcy's law (also called laminar flow)
7) Negligible gravity and capillary forces
8) Very long injection period
9) Stationary fronts of infinitesimal thickness.
10) No cross-flow between layers.
11) Single injector located at the center of the reservoir.

The mass balance on a cylindrical element of flow is written using the general continuity equation for flow in cylindrical coordinates. Steam condensation as a result of heat losses to the surroundings is included in the continuity equation using the concepts discussed in [26] and [27]. Assuming a three-region multi-layer composite reservoir model (Fig. 1), diffusivity equation for flow in the first region for any layer *i* can be written as:

$$\frac{1}{r}\frac{\partial}{\partial r}\left(r\frac{\partial p_{1i}}{\partial r}\right)=\frac{(\varphi c_t)_{1i}}{\left(\frac{k}{\mu}\right)_{1i}}\frac{\partial p_{1i}}{\partial t}+G_i\frac{(Fe-1)}{\left(\frac{k}{\mu}\right)_{1i}} \quad (1)$$

Indices 1 and i refer to the first region and the ith layer, respectively. In this model, G_i is the volume of liquid water generated by condensation per unit reservoir volume and time or rate of condensation per unit volume, described in terms of the rate of heat loss from region 1 of layer i as:

$$G_i=\frac{\left(-K\frac{\partial T}{\partial z}|z=z_i\times\pi R_{1i}^2\right)+\left(-K\frac{\partial T}{\partial z}|z=z_i+h_i\times\pi R_{1i}^2\right)}{\pi R_{1i}^2\,h_i\rho_w L_V} \quad (2)$$

Identical heat loss from top and bottom bases of the cylinder is assumed in [26] and [27], and we applied this to individual layers. The lower-bound expression given in [26] for the heat loss is applied since it can better approximate the fall-off test conditions. Therefore:

$$-K\frac{\partial T}{\partial z}\cong\frac{K}{\sqrt{\pi\alpha}}\frac{(T_s-T_i)}{\sqrt{t}} \quad (3)$$

And so, the expression for G_i becomes:

$$G_i=\frac{2K}{\sqrt{\pi\alpha}\;h_i\rho_w L_V}\frac{(T_s-T_i)}{\sqrt{t}} \quad (4)$$

Lower-bound represents the case in which temperature assumes the constant value *Ts* as soon as the steam injection begins, while the upper-bound represents a reservoir at initial temperature which reaches *Ts* as soon as the steam front arrives (there is a delay compared to the first case).

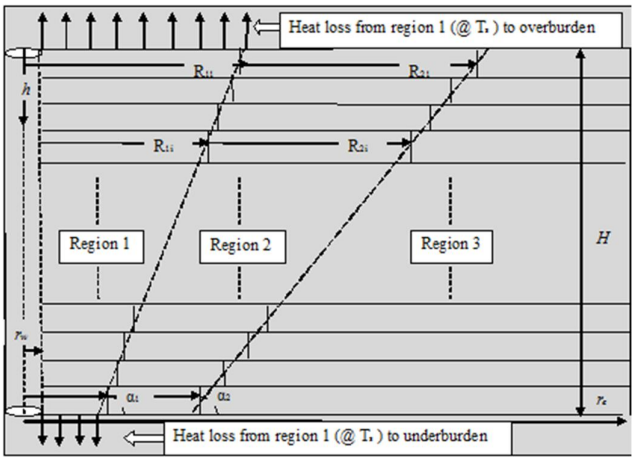

Fig. 1 Representation of the 3-region composite multi-layer reservoir model with tilted fronts and heat loss effect

In Fig. 1, the inner region is composed of a number of cylinders of varying radii stacked on top of each other. The volume of the cone frustum shown by the imaginary dashed line intersecting the layers' fronts should be equal to the volume of the cylinders. Reference [28] shows the calculations, knowing the values of the front angle, thickness, number of layers and a minimum front radius (corresponding to the bottom layer). Values of front radii corresponding to different front angles in this study result from such a volume balance calculation.

Dimensionless parameters are defined here to rewrite the equations in dimensionless form:

$$r_D=\frac{r}{r_w},\qquad p_{jiD}=\frac{2\pi\left(\frac{k}{\mu}\right)_1 H}{qB}(p_i-p_{ji})\qquad j=1,2,3$$

$$p_{wD}=\frac{2\pi\left(\frac{k}{\mu}\right)_1 H}{qB}(p_i-p_{wf}),\qquad t_D=\frac{\left(\frac{k}{\mu}\right)_1 t}{(\overline{\varphi c_t})_1 {r_w}^2}$$

$$\omega_{1i}=\frac{(\varphi c_t)_{1i}h_i}{(\overline{\varphi c_t})_1 H},\qquad \lambda_{1i}=\frac{\left(\frac{k}{\mu}\right)_{1i}h_i}{\left(\frac{k}{\mu}\right)_1 H}$$

$$\beta = \frac{4\pi(Fe-1)K(T_s-T_i)r_w}{\rho_w L_V qB}\left(\frac{\left(\frac{\overline{k}}{\mu}\right)_1}{\pi\alpha(\overline{\varphi c_t})_1}\right)^{\frac{1}{2}}$$

$$\left(\frac{\overline{k}}{\mu}\right)_1 = \frac{\sum\left(\frac{k}{\mu}\right)_{1i} h_i}{H}, \quad (\overline{\varphi c_t})_1 = \frac{\sum(\varphi c_t)_{1i} h_i}{H}, \quad H = \sum h_i$$

Dimensionless radius could be defined as $r_D = \frac{r}{R_{1i}}$. Then, instead of r_w in the definition of dimensionless parameters and in the flow equations, R_{1i} will appear. However, in this study the traditional definition of r_D is used since R_{1i} is different for each layer.

Using the definition provided for dimensionless parameters, equation 1 can be written as:

$$\frac{\partial^2 p_{1iD}}{\partial {r_D}^2} + \frac{1}{r_D}\frac{\partial p_{1iD}}{\partial r_D} = \frac{\omega_{1i}}{\lambda_{1i}}\frac{\partial p_{1iD}}{\partial t_D} - \frac{\beta}{\lambda_{1i}}\frac{1}{\sqrt{t_D}} \quad \text{for} \quad 1 < r_D < R_{1iD} \tag{5}$$

Flow in the second region of each layer is described by:

$$\frac{1}{r}\frac{\partial}{\partial r}\left(\left(\frac{k}{\mu}\right)_{2i} r\frac{\partial p_{2i}}{\partial r}\right) = (\varphi c_t)_{2i}\frac{\partial p_{2i}}{\partial t} \tag{6}$$

In this region, properties are not constant and vary exponentially with the ratio of radial distance to the first front radius at any layer as:

$$\left(\frac{k}{\mu}\right)_{2i} = \frac{\left(\frac{\overline{k}}{\mu}\right)_{1i}}{M_{12i}}\left(\frac{r}{R_{1i}}\right)^{-\theta 1}$$

In the same way, for storage in the second region:

$$(\varphi c_t)_{2i} = \frac{(\varphi c_t)_{1i}}{F_{12i}}\left(\frac{r}{R_{1i}}\right)^{-\theta 2}$$

M_{12i} and F_{12i} are mobility and storativity ratios at the first front in each layer, respectively. Equation 6 after some manipulations can be written in dimensionless form as:

$$\frac{\partial^2 p_{2iD}}{\partial {r_D}^2} + \frac{1-\theta_1}{r_D}\frac{\partial p_{2iD}}{\partial r_D} = \frac{\omega_{1i}}{\lambda_{1i}}\frac{M_{12i}}{F_{12i}}(R_{1iD})^{\theta 2-\theta 1}\, {r_D}^{\theta 1-\theta 2}\frac{\partial p_{2iD}}{\partial t_D} \quad \text{for} \quad R_{1iD} < r_D < R_{2iD} \tag{7}$$

The flow equation in the third region of each layer is:

$$\frac{1}{r}\frac{\partial}{\partial r}\left(\left(\frac{k}{\mu}\right)_{3i} r\frac{\partial p_{3i}}{\partial r}\right) = (\varphi c_t)_{3i}\frac{\partial p_{3i}}{\partial t} \tag{8}$$

Considering constant properties in this region, equation 8 is written in dimensionless form as:

$$\frac{\partial^2 p_{3iD}}{\partial {r_D}^2} + \frac{1}{r_D}\frac{\partial p_{3iD}}{\partial r_D} = \frac{\omega_{1i}}{\lambda_{1i}}\frac{M_{13i}}{F_{13i}}\frac{\partial p_{3iD}}{\partial t_D} \quad \text{for} \quad r_D > R_{2iD} \tag{9}$$

To solve the derived flow equations for different regions, initial and boundary conditions are introduced first. Initially, the system is at equilibrium or initial pressure. In dimensionless form:

$$p_{1iD} = p_{2iD} = p_{3iD} = 0 \quad @ \quad t_D = 0 \tag{10}$$

Wellbore storage is not considered in the analysis at the moment, however, effect of skin for each layer is written as:

$$p_{wD} = p_{1iD}|(r_D = 1) - Si\left(r_D\frac{\partial p_{1iD}}{\partial r_D}\right)|(r_D = 1) \tag{11}$$

Interface equations are written assuming the continuity of pressure and flux across the fronts. The continuity of pressure across the fronts is written in dimensionless form as:

$$p_{1iD} = p_{2iD} \quad @ \quad r_D = R_{1iD} \tag{12}$$

$$p_{2iD} = p_{3iD} \quad @ \quad r_D = R_{2iD} \tag{13}$$

The condition of continuity of flux across the fronts is also written in dimensionless form as:

$$M_{12i}\left(\frac{\partial p_{1iD}}{\partial r_D}\right) = \left(\frac{\partial p_{2iD}}{\partial r_D}\right) \tag{14}$$

$$M_{23i}\left(\frac{\partial p_{2iD}}{\partial r_D}\right) = \left(\frac{\partial p_{3iD}}{\partial r_D}\right) \tag{15}$$

The outer boundary condition is written for different types of boundaries in dimensionless form as:

1) Infinite-acting reservoir:

$$\lim_{r_D\to\infty} p_{3iD} = 0 \tag{16}$$

2) No-flow boundary:

$$\frac{\partial p_{3iD}}{\partial r_D}|(r_D = r_{eD}) = 0 \tag{17}$$

3) Constant-pressure boundary:

$$p_{3iD} = 0 \quad @ \quad r_D = r_{eD} \tag{18}$$

In addition to equation 11, another inner-boundary condition (including contributions from all layers) is the steam injection at constant rate (in dimensionless form):

$$\sum_i \lambda_{1i}\left(r_D\frac{\partial p_{1iD}}{\partial r_D}\right)|(r_D = 1) = -1 \tag{19}$$

The next step is to take the Laplace of the differential equations and the initial and boundary conditions in order to form a system of equations and then solve it. Taking the Laplace of equation 5 yields:

$$\frac{\partial^2 \overline{p_{1iD}}}{\partial {r_D}^2} + \frac{1}{r_D}\frac{\partial \overline{p_{1iD}}}{\partial r_D} - s\frac{\omega_{1i}}{\lambda_{1i}}\left(\overline{p_{1iD}} - \frac{\beta}{\omega_{1i}}\frac{\sqrt{\pi}}{s^{3/2}}\right) = 0 \tag{20}$$

Solution to this equation is:

$$\overline{p_{1iD}} = A_i I_0\left(\sqrt{\frac{\omega_{1i}}{\lambda_{1i}}s}\, r_D\right) + B_i K_0\left(\sqrt{\frac{\omega_{1i}}{\lambda_{1i}}s}\, r_D\right) + \frac{\beta}{\omega_{1i}}\frac{\sqrt{\pi}}{s^{3/2}} \tag{21}$$

Taking the Laplace of equation 7 gives:

$$\frac{\partial^2 \overline{p_{2iD}}}{\partial {r_D}^2} + \frac{1-\theta_1}{r_D}\frac{\partial \overline{p_{2iD}}}{\partial r_D} - \frac{\omega_{1i}}{\lambda_{1i}}\frac{M_{12i}}{F_{12i}}(R_{1iD})^{\theta 2-\theta 1}\, {r_D}^{\theta 1-\theta 2}\, s\overline{p_{2iD}} = 0 \qquad (22)$$

Solution to equation 22 is obtained by comparison with the general Bessel equation as (explained in Appendix A):

$$\overline{p_{2iD}} = C_i {r_D}^{\gamma} I_v(\xi\, {r_D}^{b}) + D_i {r_D}^{\gamma} K_v(\xi\, {r_D}^{b}) \qquad (23)$$

Taking the Laplace of equation 9 gives:

$$\frac{\partial^2 \overline{p_{3iD}}}{\partial {r_D}^2} + \frac{1}{r_D}\frac{\partial \overline{p_{3iD}}}{\partial r_D} - \frac{\omega_{1i}}{\lambda_{1i}}\frac{M_{13i}}{F_{13i}} s\overline{p_{3iD}} = 0 \qquad (24)$$

Solution to this equation is:

$$\overline{p_{3iD}} = E_i I_0\left(\sqrt{\frac{\omega_{1i}}{\lambda_{1i}}\frac{M_{13i}}{F_{13i}} s}\; r_D\right) + F_i K_0\left(\sqrt{\frac{\omega_{1i}}{\lambda_{1i}}\frac{M_{13i}}{F_{13i}} s}\; r_D\right) \qquad (25)$$

The next step is to take the Laplace of the boundary conditions discussed and substituting for the above pressure solutions (equations 21, 23, 25) in these conditions. The set of equations to be solved is:

$$\begin{gathered}
a_{11i}A_i + a_{12i}B_i - \overline{p_{wD}} = d_{1i} \\
a_{21i}A_i + a_{22i}B_i + a_{23i}C_i + a_{24i}D_i = d_{2i} \\
a_{33i}C_i + a_{34i}D_i + a_{35i}E_i + a_{36i}F_i = d_{3i} \\
a_{41i}A_i + a_{42i}B_i + a_{43i}C_i + a_{44i}D_i = d_{4i} \\
a_{53i}C_i + a_{54i}D_i + a_{55i}E_i + a_{56i}F_i = d_{5i} \\
a_{65i}E_i + a_{66i}F_i = d_{6i} \\
\textstyle\sum_i (a_{1i}A_i + a_{2i}B_i) = d_{6n+1}
\end{gathered}$$

Equations introduced above form a system of equations with contribution from all the layers which can be written in matrix form as $aX=d$. With the coefficients defined in Appendix B and the unknowns A_i to F_i and $\overline{p_{wD}}$, the system of 6n+1 equations is solved and the unknown matrix is obtained to give the wellbore pressure as well as the pressure of different regions in individual layers (in Laplace space). In this system, notice that equation 11 for each layer is written in such a way that $\overline{p_{wD}}$ is the $(6n+1)^{th}$ unknown which is directly obtained from the solution of the system of equations where n is the number of layers. The last equation in this system contains contribution from all layers in a single equation. This is obtained by taking the Laplace of equation 19 and substituting for p_{1iD}.

To obtain the dimensionless wellbore pressure and pressure derivative, the last unknown, $\overline{p_{wD}}$ is inverted numerically from Laplace space to real space by Stehfest algorithm [29]. Wellbore pressure obtained does not include any wellbore storage effect. To include this effect in the solution, procedure of [30] is applied as:

$$\overline{p_{wD}} = \frac{1}{C_D s^2 + \dfrac{1}{\overline{p_{wD}}_{CD=0}}} \qquad (26)$$

This equation is again numerically inverted to obtain the dimensionless wellbore pressure and pressure derivative including wellbore storage and skin.

Decline curve analysis for the proposed model can also be done. If the inner boundary condition is constant pressure injection at wellbore, the injection rate varies. In this case, variation of rate with time is of interest. Reference [30] suggested that the solution is related to the previously obtained constant rate solution using the superposition principle. This issue is not discussed further in this paper.

III. Results and Discussion

A. Model Verification

The model presented in the previous section is validated against some of the traditional composite reservoir models. The new model will repeat these models by setting values to the parameters of the model.

Notice that if $\omega_{1i} = \lambda_{1i} = 1$ and index i is dropped; the equations represent the single layer reservoir model. The model will reproduce the model of [14] by setting heat loss coefficient (β) to zero and assuming vertical fronts (either by assigning identical front radii to all layers or by using a single layer model). This model will further reproduce many of the two-region composite models such as [3] and [31]. To generate the two-region models, R_{2D} is set equal to R_{1D} and fronts are assumed vertical. θ_1 and θ_2 are set to zero to model constant properties in the two regions. Fig. 2 shows the derivative response for different values of mobility ratio between the two regions.

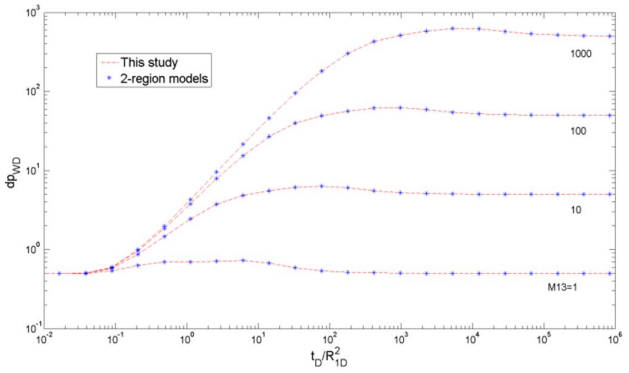

Fig. 2 Comparison of this study with 2-region composite reservoir models, C_D=0; S=0; R_{1D}=R_{2D}=500; M_{12}=1; F_{13}=10; F_{12}=1

The model will further reproduce three-region composite models such as [7] and [31]. Exponents θ_1 and θ_2 are set to zero to model constant properties in the regions. Fig. 3 shows the perfect match for different storativity ratios.

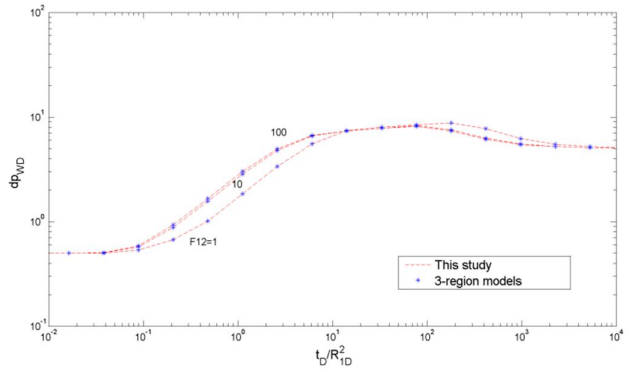

Fig. 3 Comparison of this study with 3-region composite reservoir models, C_D=0; S=0; R_{1D}=500; R_{2D}=750; M_{12}=5; M_{13}=10; F_{13}=100

The model also matches the model of [27] including the heat loss effect. This effect is discussed later in this paper. Effect of gravity is usually investigated by multi-layer models, such as in [16] or [17]. Fig. 4 shows a perfect match between this study and the multi-layer composite model of [16]-[19] and also [20] assuming negligible cross-flow, with tilted front.

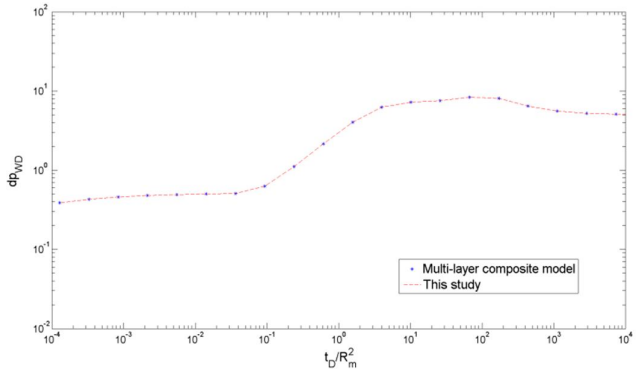

Fig. 4 Comparison of this study with multi-layer composite reservoir model of [16]-[20], C_D=0; S=0; R_m=200; M=10; F=100; α=60°; N=3

Fig. 5 shows the reproduction of the pressure and derivative responses of the commingled multi-layer model of [16] by the model presented in this work, using data of Table 1 of [16].

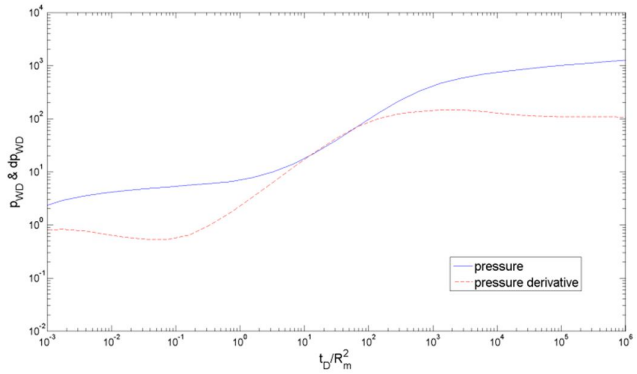

Fig. 5 Reproduction of the multi-layer composite model of [16], C_D= 31.64; S=0; R_m=440; M=213; F=18; α=60°; N=2

B. Sensitivity Analysis

Effects of the parameters such as mobility and storage ratios on the pressure behaviour are not discussed here (reader is referred to [7] or [31] for detailed discussion as the same conclusions are valid for this study). Effect of other parameters like heat loss, gravity, size of regions, and variation of properties on the pressure response is investigated in this section.

Unless mentioned, the following parameters are used in the generation of pressure responses:

C_D=0; S=0; R_m=500; M_{12}=10; M_{13}=1000; F_{12}=10; F_{13}=500; α=60; β=0; $\theta_1=\theta_2$=1; N=6; λ_{1i}=0.1666; ω_{1i}=0.1666; H_D=100.

In this paper, dp_{WD} refers to the logarithmic pressure derivative or $dp_{WD}/dlnt_D$. The value of 0.5 on derivative plot refers to the initial radial flow in the inner region. As can be observed from the equations, average properties of the inner region are used in the definition of dimensionless parameters. Late time derivative stabilization refers to the radial flow in the outer region.

1) Effect of Heat Loss

The model presented in [27] includes heat loss effect and concludes that under certain conditions, heat loss could have a significant effect on the pressure behavior and dominate the flow regimes. It is shown in Fig. 6 that for low values of β, pressure responses are similar. However, higher values of β cause some deviation due to significant heat loss as observed here for the β of 0.1.

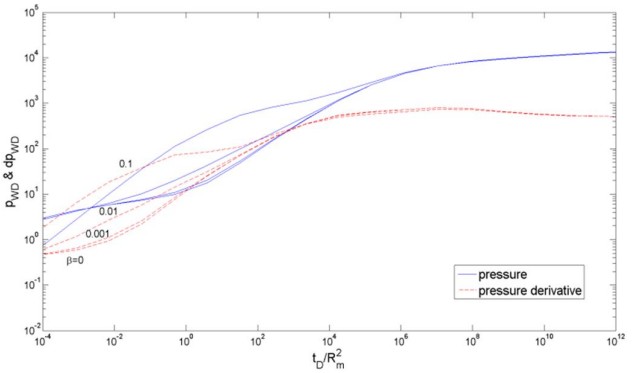

Fig. 6 Pressure and derivative responses for different values of heat loss coefficient, H_D=30; R_m=200

A half slope line on log-log plots of pressure and derivative responses appear for higher values of β which is similar to the response of linear flow. The effect is not significant on the late time response due to huge mobility decrease in the outer region and domination of mobility term, as shown in Fig. 6.

2) Effect of Gravity

As mentioned in the previous section, gravity is usually modeled using the concept of multi-layered models (for instance in [16]-[20]). This requires setting different values of radii to fronts at each layer.

Fig. 7 shows the effect of front angle on pressure derivative plot. As the gravity effect becomes more significant or the front angle gets smaller, average front radius becomes larger and pressure has more time to diffuse in the inner region resulting in a longer initial radial flow and delayed deviation due to the second region. Huge gravity may even delay the occurrence of the transition hump and the last radial flow.

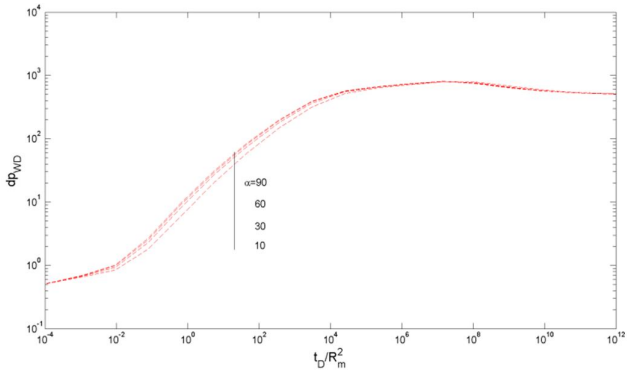

Fig. 7 Effect of the front angle

Fig. 8 shows derivative responses generated for different values of thickness. A thicker formation will exhibit more gravity override. The expected trend similar to that seen in Fig. 7 also appears here. Again, longer initial radial flow is established for more significant gravity effect.

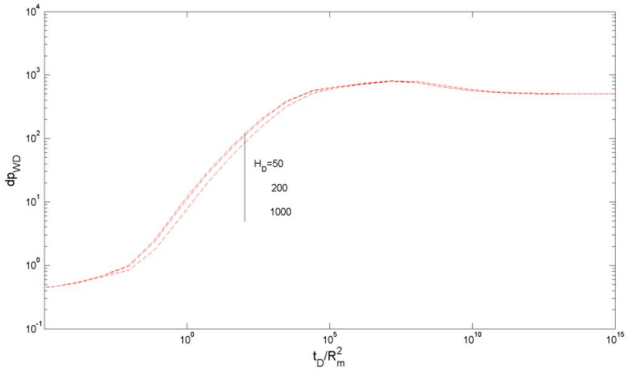

Fig. 8 Effect of formation thickness

The number of layers used to build the model does not change the pressure responses as shown in Fig. 9

3) Effect of the Intermediate Region

Effect of the relative size of the intermediate region compared to the inner region is analyzed using the parameter r_{f2}/r_{f1} in Fig. 10. This parameter is the ratio of the second to the first front radius (assumed to be the same for different layers) or a measure of the volume ratio.

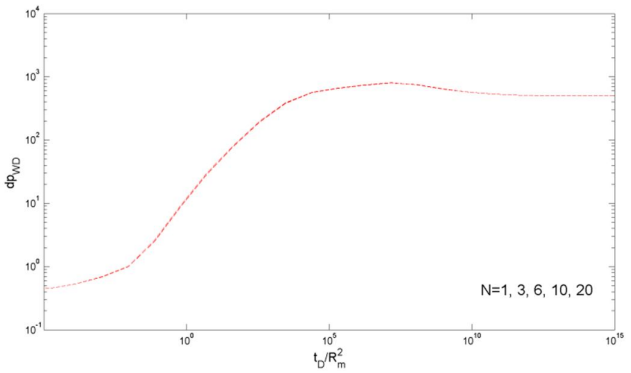

Fig. 9 Effect of the number of layers

Larger size highly affects the middle-time response. It will show longer transition response and therefore delayed radial flow response from the outer region. It will also result in more deviation from the PSS flow regime as the corresponding transition unit slope line gradually disappears.

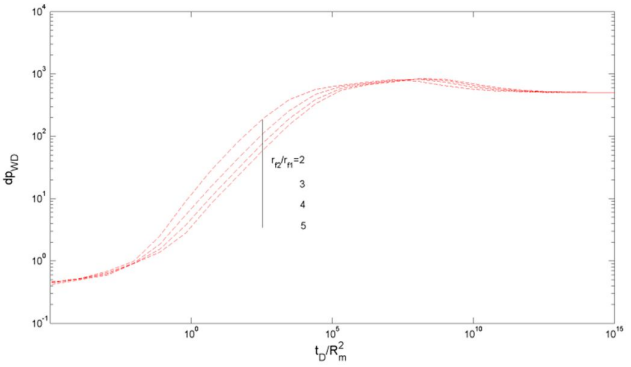

Fig. 10 Effect of the size of the intermediate region

As shown in Fig. 11, larger value of minimum front radius (R_m) or in another words, a bigger inner region obviously results in longer inner region radial flow and delayed intermediate and outer region responses.

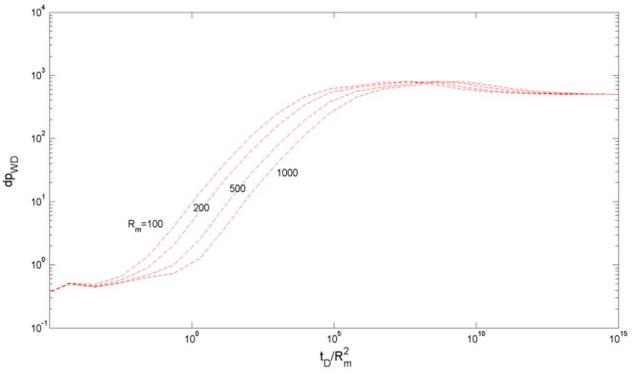

Fig. 11 Effect of the minimum front radius

Mobility and storativity in the intermediate region change with radial distance in a power-law fashion. As shown in Fig. 12, value of mobility exponent (θ_1) does not have an effect on the early response from the intermediate region. However, after this short period, deviation from the early response happens and the observed trend shows smooth and longer transition pressure curves for increased values of θ_1. Smooth transition from the inner to the outer region indicates deviation from the PSS behavior. In fact, smooth decline of properties in the proposed model dampens the sharp property variation assumption of the PSS method.

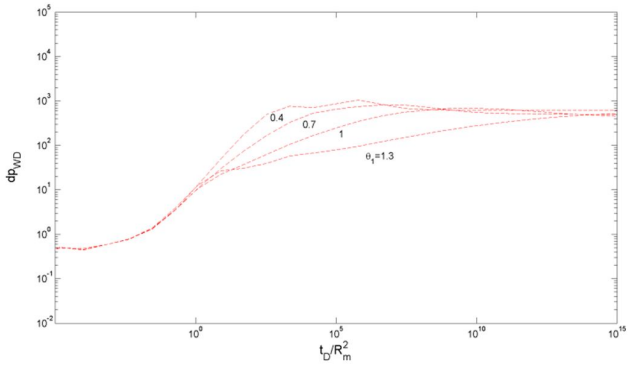

Fig. 12 Effect of the variation of mobility, H_D=30; R_m=200

Effect of the storativity exponent (θ_2) is shown in Fig. 13. The general trend and conclusion of Fig. 12 is valid for Fig. 13, as well. Deviation from the PSS behavior happens for smooth property variations (or increased value of exponent).

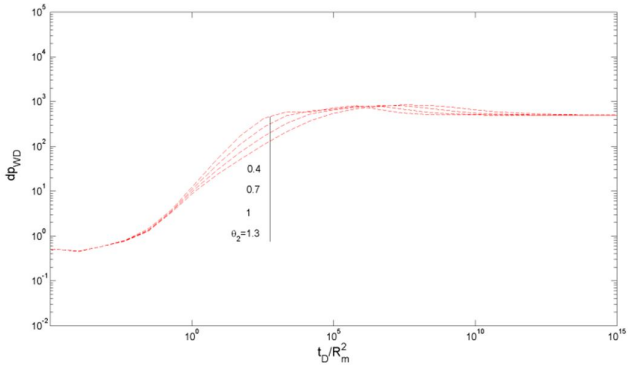

Fig. 13 Effect of the variation of storativity, H_D=30; R_m=200

4) Effect of the Boundary

So far in this paper, infinite–acting reservoir model was used for the analysis. As presented in Appendix B, solutions for bounded reservoirs are also obtained using the corresponding coefficients. Fig. 14 shows the pressure and pressure derivative responses for both infinite-acting reservoir and no-flow boundaries for several values of external radius. Late time derivative response for infinite-acting model follows a horizontal (constant value) pattern. For the closed reservoir, pressure and pressure derivative curves are the same as the infinite model as long as the effect of the no-flow boundary is not felt (transient state). When the pressure waves hit the first reservoir boundary, response starts to deviate from the infinite model. After pressure waves hit all the reservoir boundaries and entering the PSS flow regime, pressure and pressure derivative curves converge and exhibit unit slope lines on log-log plot at late times. This behaviour is delayed for larger reservoirs.

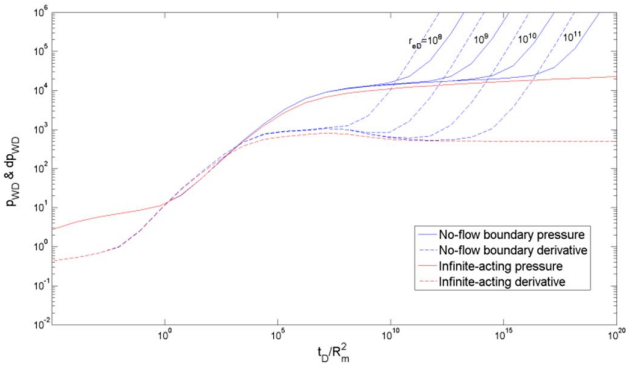

Fig. 14 Comparison of the infinite-acting and closed reservoir models

Constant-pressure boundary model response is compared with the infinite and closed reservoir models in Fig. 15. For this model, again response is similar to infinite-acting model until effects of the boundaries are felt. Thereafter, steady-state flow regime is established because of the pressure support of the boundaries. Steady-state condition causes the pressure derivative to decline towards zero at late times.

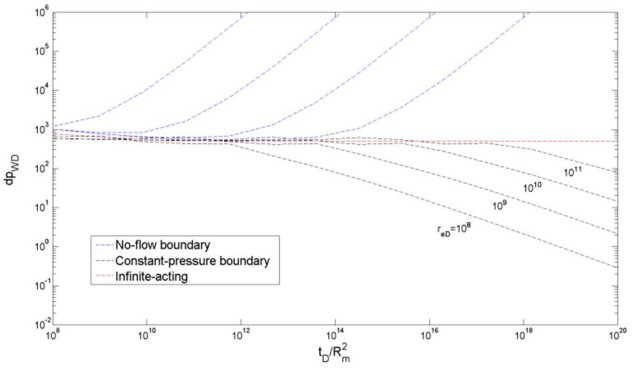

Fig. 15 Comparison of the infinite-acting, no-flow, and constant-pressure boundary models

IV. Conclusions

In this paper, an analytical three-region model for well test analysis of composite reservoirs including heat loss and gravity effects was proposed which is considered an improvement over the traditional two-region models. Different types of bounded and unbounded reservoir models are considered. The model was verified using some of the

conventional models. It can explain some of the anomalies seen on the pressure data.

Heat loss to the formation can distort the pressure behavior. This effect may be misinterpreted as linear flow due to the presence of fractures or channel flow, since the corresponding heat loss term in the pressure equations takes the mathematical form of the linear flow. This can cause errors in the interpretation and calculations.

The intermediate region included in the model is assigned a continuous decline of properties with distance that will prevent abrupt changes and abnormal pressure responses at the front location. The reservoir model is assigned tilted fronts due to gravity override. Generally, gravity effect results in longer radial flow from the inner region. If significant, it can also cause delays in the occurrence of the middle and late time responses. Increase in the relative size of the intermediate region considered in this study can result in a longer transition response and delayed late time radial flow.

Application of the PSS method for volume estimation should be reconsidered for the conditions that cause deviation from this simple behavior. Several cases discussed in this work show smooth transition from the inner to the outer region. These include increased size of the intermediate region and continuous decline of properties in this region that in fact dampen the assumption of sharp variations in PSS method due to the presence of the intermediate region. Type curve matching method using the parameters discussed in the development of the model can serve as an alternative for reservoir characterization to obtain better estimates. The model developed in this study can be further applied to include other types of composite reservoirs.

ACKNOWLEDGMENT

Authors would like to gratefully thank the Department of Petroleum Engineering and Applied Geophysics at NTNU (Trondheim) for all the support for doing this research. Professor Jon Kleppe is appreciated for his valuable comments and review. Financial support from Statoil ASA is highly appreciated.

NOMENCLATURE

B	Formation volume factor, m^3/Sm^3
c_t	Total compressibility, Pa^{-1}
C_D	Dimensionless wellbore storage coefficient
F	Storativity ratio at the front between different regions
F_ρ	Density ratio of water to steam, dimensionless
G	Rate of steam condensation, $m^3/ (s.m^3)$
H	Thickness of the reservoir, m
k	Permeability, m^2
K	Thermal conductivity, W/(m.K)
M	Mobility ratio at the front between different regions
p	Pressure, Pa
p_D	Dimensionless pressure change
p_i	Initial reservoir pressure, Pa
q	Injection (production) flow rate, Sm^3/s
R	Front radius, m
r_D	Dimensionless radial distance
r_e	External boundary radius, m
r_w	Wellbore radius, m
s	Laplace variable
S	Skin factor, dimensionless
t	Time, s
t_D	Dimensionless time
T	Temperature, K
T_R	Reservoir temperature, K
T_S	Steam temperature, K

Greek Letters

α	Thermal diffusivity, m^2/sec
β	Steam condensation coefficient, dimensionless
θ_1	Exponent for mobility variation
θ_2	Exponent for storativity variation
λ	Relative mobility, dimensionless
μ	Viscosity, Pa.s
ρ	Density, kg/m^3
φ	Porosity, fraction
ω	Relative storativity, dimensionless

APPENDIX A: DEVELOPMENT OF THE SOLUTION TO FLOW EQUATION IN THE INTERMEDIATE REGION

A solution to equation 22 is obtained by comparison with the solution for the general Bessel equation. The general Bessel equation in Laplace space is given in [32] as:

$$\frac{d^2\overline{y}}{dx^2} + \frac{n}{x}\frac{d\overline{y}}{dx} - \frac{q^2}{x^{n-m}}\overline{y} = 0$$

A solution to this equation is:

$$\overline{y} = Ax^{-\frac{1}{2}(n-1)}K_v\left(\frac{2q}{m-n+2}x^{-\frac{1}{2}(m-n+2)}\right) + Bx^{-\frac{1}{2}(n-1)}I_v\left(\frac{2q}{m-n+2}x^{-\frac{1}{2}(m-n+2)}\right)$$

Where

$$v = \frac{1-n}{m-n+2}$$

Comparison of equation 22 with the general Bessel equation yields:

$$\overline{p_{2iD}} \equiv \overline{y} \qquad r_D \equiv x \qquad 1-\theta_1 \equiv n$$

$$\frac{\omega_{1i}}{\lambda_{1i}}\frac{M_{12i}}{F_{12i}}(R_{1iD})^{\theta 2-\theta 1}\, s \equiv q^2 \qquad 1-\theta_2 \equiv m$$

The equivalent solution to equation 22 is therefore:

$$\overline{p_{2iD}} = C_i {r_D}^{\gamma} I_v(\xi\, {r_D}^{b}) + D_i {r_D}^{\gamma} K_v(\xi\, {r_D}^{b})$$

Where

$$\gamma = \frac{\theta_1}{2} \qquad b = \frac{\theta_1-\theta_2+2}{2}$$

$$v = \frac{\theta_1}{\theta_1 - \theta_2 + 2} \qquad \xi = \sqrt{\frac{\omega_{1i}}{\lambda_{1i}} \frac{M_{12i}}{F_{12i}} s} \; \frac{\sqrt{(R_{1iD})^{\theta_2 - \theta_1}}}{b}$$

APPENDIX B: MATRIX OF COEFFICIENTS FOR PRESSURE SOLUTION

Taking the Laplace of boundary conditions introduced in the description of the model, the elements of the matrix of coefficients are written as:

$$a_{11i} = I_0\left(\sqrt{\frac{\omega_{1i}}{\lambda_{1i}} s}\right) - S_i \sqrt{\frac{\omega_{1i}}{\lambda_{1i}} s} \; I_1\left(\sqrt{\frac{\omega_{1i}}{\lambda_{1i}} s}\right)$$

$$a_{12i} = K_0\left(\sqrt{\frac{\omega_{1i}}{\lambda_{1i}} s}\right) + S_i \sqrt{\frac{\omega_{1i}}{\lambda_{1i}} s} \; K_1\left(\sqrt{\frac{\omega_{1i}}{\lambda_{1i}} s}\right)$$

$$a_{6n+1} = -1$$

$$a_{21i} = I_0\left(\sqrt{\frac{\omega_{1i}}{\lambda_{1i}} s} \; R_{1iD}\right)$$

$$a_{22i} = K_0\left(\sqrt{\frac{\omega_{1i}}{\lambda_{1i}} s} \; R_{1iD}\right)$$

$$a_{23i} = -R_{1iD}{}^{\gamma} I_v\left(\xi \; R_{1iD}{}^{b}\right)$$
$$a_{24i} = -R_{1iD}{}^{\gamma} K_v\left(\xi \; R_{1iD}{}^{b}\right)$$
$$a_{33i} = R_{2iD}{}^{\gamma} I_v\left(\xi \; R_{2iD}{}^{b}\right)$$
$$a_{34i} = R_{2iD}{}^{\gamma} K_v\left(\xi \; R_{2iD}{}^{b}\right)$$

$$a_{35i} = -I_0\left(\sqrt{\frac{\omega_{1i}}{\lambda_{1i}} \frac{M_{13i}}{F_{13i}} s} \; R_{2iD}\right)$$

$$a_{36i} = -K_0\left(\sqrt{\frac{\omega_{1i}}{\lambda_{1i}} \frac{M_{13i}}{F_{13i}} s} \; R_{2iD}\right)$$

$$a_{41i} = M_{12i} \sqrt{\frac{\omega_{1i}}{\lambda_{1i}} s} \; I_1\left(\sqrt{\frac{\omega_{1i}}{\lambda_{1i}} s} \; R_{1iD}\right)$$

$$a_{42i} = -M_{12i} \sqrt{\frac{\omega_{1i}}{\lambda_{1i}} s} \; K_1\left(\sqrt{\frac{\omega_{1i}}{\lambda_{1i}} s} \; R_{1iD}\right)$$

$$a_{43i} = -\left[\gamma R_{1iD}{}^{\gamma-1} I_v\left(\xi \; R_{1iD}{}^{b}\right) + \xi b \; R_{1iD}{}^{\gamma+b-1} \acute{I}_v\left(\xi \; R_{1iD}{}^{b}\right)\right]$$
$$a_{44i} = -\left[\gamma R_{1iD}{}^{\gamma-1} K_v\left(\xi \; R_{1iD}{}^{b}\right) + \xi b \; R_{1iD}{}^{\gamma+b-1} \acute{K}_v\left(\xi \; R_{1iD}{}^{b}\right)\right]$$
$$a_{53i} = M_{23i}\left[\gamma R_{2iD}{}^{\gamma-1} I_v\left(\xi \; R_{2iD}{}^{b}\right) + \xi b \; R_{2iD}{}^{\gamma+b-1} \acute{I}_v\left(\xi \; R_{2iD}{}^{b}\right)\right]$$
$$a_{54i} = M_{23i}\left[\gamma R_{2iD}{}^{\gamma-1} K_v\left(\xi \; R_{2iD}{}^{b}\right) + \xi b \; R_{2iD}{}^{\gamma+b-1} \acute{K}_v\left(\xi \; R_{2iD}{}^{b}\right)\right]$$

$$a_{55i} = -\sqrt{\frac{\omega_{1i}}{\lambda_{1i}} \frac{M_{13i}}{F_{13i}} s} \; I_1\left(\sqrt{\frac{\omega_{1i}}{\lambda_{1i}} \frac{M_{13i}}{F_{13i}} s} \; R_{2iD}\right)$$

$$a_{56i} = \sqrt{\frac{\omega_{1i}}{\lambda_{1i}} \frac{M_{13i}}{F_{13i}} s} \; K_1\left(\sqrt{\frac{\omega_{1i}}{\lambda_{1i}} \frac{M_{13i}}{F_{13i}} s} \; R_{2iD}\right)$$

For infinite-acting reservoir:

$$a_{65i} = a_{66i} = 0$$

For no-flow boundary:

$$a_{65i} = I_1\left(\sqrt{\frac{\omega_{1i}}{\lambda_{1i}} \frac{M_{13i}}{F_{13i}} s} \; r_{eD}\right)$$

$$a_{66i} = -K_1\left(\sqrt{\frac{\omega_{1i}}{\lambda_{1i}} \frac{M_{13i}}{F_{13i}} s} \; r_{eD}\right)$$

For constant-pressure boundary:

$$a_{65i} = I_0\left(\sqrt{\frac{\omega_{1i}}{\lambda_{1i}} \frac{M_{13i}}{F_{13i}} s} \; r_{eD}\right)$$

$$a_{66i} = K_0\left(\sqrt{\frac{\omega_{1i}}{\lambda_{1i}} \frac{M_{13i}}{F_{13i}} s} \; r_{eD}\right)$$

The elements of matrix *d* are written as:

$$d_{1i} = -\frac{\beta}{\omega_{1i}} \frac{\sqrt{\pi}}{s^{3/2}}$$

$$d_{2i} = -\frac{\beta}{\omega_{1i}} \frac{\sqrt{\pi}}{s^{3/2}}$$

$$d_{3i} = 0$$
$$d_{4i} = 0$$
$$d_{5i} = 0$$
$$d_{6i} = 0$$

For the last equation of the system we have:

$$\sum_i (a_{1i} A_i + a_{2i} B_i) = d_{6n+1}$$

where

$$a_{1i} = \sqrt{\lambda_{1i} \omega_{1i}} \; I_1\left(\sqrt{\frac{\omega_{1i}}{\lambda_{1i}} s}\right)$$

$$a_{2i} = -\sqrt{\lambda_{1i} \omega_{1i}} \; K_1\left(\sqrt{\frac{\omega_{1i}}{\lambda_{1i}} s}\right)$$

$$d_{6n+1} = -\frac{1}{s^{3/2}}$$

REFERENCES

[1] W. Hurst, "Interference between oil fields," *Trans., AIME*, vol. 219, pp. 175-192, 1960.

[2] R. D. Carter, "Pressure Behavior of a Limited Circular Composite Reservoir," *SPE J.* vol. 6(4) pp. 328-34, 1966. http://dx.doi.org/10.2118/1621-PA

[3] A. Satman, M. Eggenschwiler, R. W-K. Tang, and H. J. Ramey Jr., "An Analytical Study of Transient Flow in Systems with Radial Discontinuities," in *the 55th Annual Meeting of SPE of AIME, Dallas, Texas*, 21-24 September, 1980, paper SPE 9399. http://dx.doi.org/10.2118/9399-MS

[4] H. Kazemi, "Locating a burning front by pressure transient measurements," *Journal of Petroleum Technology*, vol. 18(2), pp. 227-232, 1966. http://dx.doi.org/10.2118/1271-PA

[5] M. O. Onyekonwu, H. J. Ramey Jr., W. E. Brigham, and R. M. Jenkins, "Interpretation of Simulated Falloff Tests," in *the California Regional Meeting of SPE of AIME, Long Beach, California*, 11-13 April, 1984, paper SPE 12746. http://dx.doi.org/10.2118/12746-MS

[6] J. Barua and R. N. Horne, "Computerized Analysis of Thermal Recovery Well Test Data," *SPE Formation Evaluation Journal*, vol. 2(4), pp. 560-66, 1987. http://dx.doi.org/10.2118/12745-PA

[7] A.K. Ambastha and H. J. Ramey Jr., "Pressure Transient Analysis for a Three- Region Composite Reservoir," in *the Rocky Mountain Regional Meeting of SPE of AIME, Casper, Wyoming*, 1992, paper SPE 24378 http://dx.doi.org/10.2118/24378-MS

[8] T. Nanba and R. N. Horne, "Estimation of Water and Oil Relative Permeabilities from Pressure Transient Analysis of Water Injection Well Data," in *the Annual Technical Conference and Exhibition of SPE of AIME, San Antonio, Texas*, 8-11 October, 1989, paper SPE 19829. http://dx.doi.org/10.2118/19829-MS

[9] M. Abbaszadeh and M. Kamal, "Pressure Transient Testing of Water Injection Wells," *SPE Res. Eng.*, vol. 4(1), pp. 115-124, 1989. http://dx.doi.org/10.2118/16744-PA

[10] R. B. Bratvold and R. N. Horne, "Analysis of Pressure Falloff Tests following Cold Water Injection," *SPE Formation Evaluation Journal*, vol. 5(3) pp. 293-302, 1990. http://dx.doi.org/10.2118/18111-PA

[11] L.G. Acosta and A.K. Ambastha, "Thermal Well Test Analysis Using an Analytical Multi-Region Composite Reservoir Model," in *the Annual Technical Conference and Exhibition of SPE of AIME, New Orleans, Louisiana*, September 25-28, 1994, paper SPE 28422 http://dx.doi.org/10.2118/28422-MS

[12] C. Chakrabarty, "Pressure Transient Analysis of Non- Newtonian Power Law Fluid Flow in Fractal Reservoirs," PhD Thesis, University of Alberta, Edmonton, Alberta, April 1993.

[13] D. Poon, "Transient Pressure Analysis of Fractal Reservoirs," in *the Annual Technical Meeting of the Petroleum Society of Canada, Calgary, Alberta*, June 7-9, 1995, paper PETSOC 95-34. http://dx.doi.org/10.2118/95-34

[14] M. B. Issaka and A. K. Ambastha, "An Improved Three-region Composite Reservoir Model for Thermal Recovery Well Test Analysis," in *the Annual Meeting of CIM, Calgary, Alberta*, June 8-11, 1997, paper CIM 97-55. http://dx.doi.org/10.2118/97-55

[15] H. C. Lefkovits, P. Hazebroek, E. E. Allen, and C. S. Matthews, "A study of the behavior of bounded reservoirs composed of stratified layers," *SPE J.*, vol. 1(1), pp. 43–58, 1961. http://dx.doi.org/10.2118/1329-G

[16] A. Satman, "An Analytical Study of Transient Flow in Stratified Systems with Fluid Banks," in *SPE Annual Technical Conference and Exhibition, San Antonio, Texas*, 4-7 October, 1981, paper SPE 10264. http://dx.doi.org/10.2118/10264-MS

[17] A. Satman, and M. M. Oskay, "Effect of a Tilted Front on Well Test Analysis," paper SPE 14701 available from SPE, 1985.

[18] D.G. Hatzignatiou, D.O. Ogbe, K. Dehghani, and M.J. Economides, "Interference Pressure Behavior in Multilayered Composite Reservoirs," in *SPE Annual Technical Conference and Exhibition, Dallas, Texas*, 27-30 September, 1987, paper SPE-16766. http://dx.doi.org/10.2118/16766-MS

[19] K. Anbarci, A. S. Grader, and T. Ertekin, "Determination of Front Locations in a Multilayer Composite Reservoir," in *SPE Annual Technical Conference and Exhibition, San Antonio, Texas*, 8-11 October, 1989, paper SPE-19799. http://dx.doi.org/10.2118/19799-MS

[20] E. Gomes and A. K. Ambastha, "An Analytical Pressure-Transient Model for Multilayered, Composite Reservoirs with Pseudosteady-State Formation Crossflow," in *SPE Western Regional Meeting, Anchorage, Alaska*, 26-28 May, 1993, paper SPE-26049. http://dx.doi.org/10.2118/26049-MS

[21] J. Rabb, and C. Palmgren, "Pressure Transient Analysis in SAGD," in *Canadian International Petroleum Conference, Calgary, Canada*, 10-12 June, 2003, paper CIPC 2003-120. http://dx.doi.org/10.2118/2003-120

[22] A. Shamila, E. Shirif, M. Dong, and A. Henni, "Chamber Volume/Size Estimation for SAGD Process from Horizontal Well Testing," in *56th Annual Technical Meeting of Canadian International Petroleum Conference, Calgary, Alberta, Canada*, 7-9 June, 2005, paper CIPC 2005-075. http://dx.doi.org/10.2118/2005-075

[23] A. Jahanbani G., T. A. Jelmert, J. Kleppe, M. Ashrafi, Y. Souraki, and O. Torsaeter, "Investigation of the applicability of thermal well test analysis in steam injection wells for Athabasca heavy oil," in *EAGE Annual Conference & Exhibition incorporating SPE Europec, Copenhagen, Denmark*. 4-7 June, 2012, paper SPE 154182. http://dx.doi.org/10.2118/154182-MS

[24] A. Jahanbani G., T. A. Jelmert, and J. Kleppe, "Investigation of thermal well test analysis for horizontal wells in SAGD process," in *SPE Annual Technical Conference and Exhibition (ATCE), San Antonio, USA*, 8-10 October, 2012, paper SPE 159680. http://dx.doi.org/10.2118/159680-MS

[25] A. Jahanbani G. and J. Kleppe, "Analysis of Heat Loss Effects on Thermal Pressure Falloff Tests," in *the 14th European Conference on the Mathematics of Oil Recovery, Catania, Sicily, Italy*, 8-11 September, 2014, paper EAGE- Mo P23. DOI: 10.3997/2214-4609.20141806

[26] Y. C. Yortsos, "Distribution of fluid phases within the steam zone in steam-injection processes," *SPE Journal*, vol. 24(4), pp. 458-466, 1984. http://dx.doi.org/10.2118/11273-PA

[27] J. F. Stanislav, C. V. Easwaran, and S. L. Kokal, "Interpretation of thermal well falloff testing," *SPE Formation Evaluation Journal*, vol. 4(2), pp. 181-186, 1989. http://dx.doi.org/10.2118/16747-PA

[28] I. Kiome, "Pressure Transient Behaviour for a Well in a Multi-layered Composite Reservoir with an Inclined," M.Sc. Thesis, University of Alberta, Edmonton, Canada, 1991.

[29] H. Stehfest, "Algorithm 368: numerical inversion of Laplace transform," *Commun. Assoc. Comput. Math.*, vol. 13(1), pp. 47–49, 1970.

[30] A. F. van Everdingen and W. Hurst, "The application of the Laplace transformation to flow problems in reservoirs," *JPT*, vol. 1(12), pp. 305–324, 1949. http://dx.doi.org/10.2118/949305-G

[31] A. K. Ambastha, "Pressure Transient Analysis for Composite Systems," PhD Thesis, Stanford University, Stanford, USA, 1988.

[32] H. S. Carslaw and J. C. Jaeger, *Conduction of Heat in Solids*. London, UK: Oxford University Press, 1959.